# Modeling a Smooth Surface by a Constrained Biharmonic Equation with Application in Soil Science\*

Samson Seifu Bekele<sup>1</sup>, Maregnesh Mechal Wolde<sup>1</sup>, Claus Führer<sup>2</sup>, Nils-Otto Kitterød<sup>3</sup>, and Anne Kværnø<sup>5</sup>

<sup>1</sup>Department of Mathematics, Hawassa University, Hawassa, Ethiopia

- <sup>2</sup>Center for Mathematical Sciences, Lund University (LU), Lund, Sweden
- <sup>3</sup> Soil and Water Science Section, Norwegian University of Life Sciences (NMBU), Ås, Norway
- <sup>4</sup> Department of Mathematical Sciences, Norwegian University of Science and Technology (NTNU), Trondheim, Norway

### Abstract

This paper presents a method for mathematical modelling of surfaces conditioned on empirical data. It is based on solving a discrete biharmonic equation over a domain with given inner point and inner curve data. The inner curve data is used to model boundary values while the inner point data is used for modeling a load vector with the goal to generate a smooth surface. The construction of boundary data is an ill-posed problem, for which a special regularization approach is suggested.

The method is designed for surface construction problems with a very limited amount of measured data. In the paper we apply the method by using empirical data of soil thickness and geological maps indicating exposed bedrock regions.

### 1 Introduction

This paper deals with constructing a surface over a 2D domain from boundary data, point data and data on curves inside the domain. Surface reconstruction is an important topic in many applications and related tools are often bound to

<sup>\*</sup>Supported by NORPART-2021/10167 Ethiopian Norwegian Network in Computational Mathematics (ENNCoMat).

specific mathematical models for the application at hand. Smoothness requirements, free parameters for adapting the final shape to given data or the need for compensation for lack of data are often criteria for the design of a mathematical surface model.

There are various ways to choose surface models. In computer aided graphical design (CAGD) the models are based on function classes like splines and NURBS [16]. In CAGD given data points usually determine the free function coefficients. If the number of given data points fits the dimension of the function space, the surface construction is a 2D-interpolation problem. In the case that more data is given, surface construction leads to a fitting problem. Spline or NURBS function spaces are chosen such that data change affects the surface only locally.

In the current study we consider situations where much less data is available. This is the case in the guiding example from soil science where soil thickness has to be shaped based on very little data from occasional drilling down to the bedrock. The approach we consider for this case is based on filling the missing data by using a smooth surface model generated as a solution of a discretized partial differential equation (PDE). Typically, load functions and boundary values are used to shape the surface. In this paper we propose a method for the case when additionally point data or data from interior curves is available and when boundary data is not completely known. A PDE-based model allows the use of well-established numerical tools and software and is suited for irregular domains with non uniformly distributed measurements. An example of such an approach, based on the Poisson equation, is found in [9]. A nonlinear PDE-based method, as discussed in [4], utilizes the level set approach, where a higher-dimensional scalar function, known as the level set function, evolves according to the PDE. This function implicitly represents the surface through its zero level curve, ensuring the reconstruction of a smooth and regular surface that closely aligns with the sampled data points.

Inspired by plate bending problems in solid mechanics, we present in this paper the use of the discretized biharmonic equation to model surfaces and apply the virtual element method to define the discrete model space. The approach is demonstrated through the example of determining soil thickness over a specific geographical region. The biharmonic equation requires boundary data like position, derivative information, and load data over the entire domain. In surface reconstruction, this data is often not directly available and is instead used as modeling parameters to create surfaces with a desired shape, such as interpolating specific points, containing given lines, or meeting certain constraints. The paper takes up the following aspects: the formulation of the mathematical problem, the presentation of a guiding application, modeling alternatives, solution methods and a brief summary of the results.

### 1.1 Problem description

Our main objective is to construct the surface under consideration as the solution of a certain discretized biharmonic equation. The domain, the load vector and the boundary conditions of this biharmonic equation serve as modeling parameters to shape this surface in a way that given measurement data is taken into account. For this end we consider the following problem on a closed domain  $\Omega \subset \mathbb{R}^2$ :

$$\Delta^2 u = q \text{ in } \Omega \tag{1a}$$

with boundary conditions

$$u = f$$
 and  $\partial_n u = h$  on  $\partial \Omega_D$ , (1b)  
 $\Delta u = 0$  and  $\partial_n (\Delta u) = 0$  on  $\partial \Omega_N$ . (1c)

$$\Delta u = 0$$
 and  $\partial_n(\Delta u) = 0$  on  $\partial \Omega_N$ . (1c)

The boundary  $\partial\Omega = \partial\Omega_D \cup \partial\Omega_N$  is divided into a part  $\partial\Omega_D$  for Dirichlet boundary conditions and another  $\partial\Omega_N$  for Neumann boundary conditions. The right hand side function q will be referred to as the load function.

Given the Sobolev space  $\mathcal{H}^2(\Omega)$  and the subspace

$$\mathcal{H}_{\mathrm{D}}^{2}(\Omega) = \{ v \in \mathcal{H}^{2}(\Omega) \colon v|_{\partial\Omega_{\mathrm{D}}} = 0, (\partial_{n}v)|_{\partial\Omega_{\mathrm{D}}} = 0 \},$$

the variational formulation of (1) is:

Find  $u \in \mathcal{H}^2(\Omega)$  satisfying the boundary conditions (1b) and (1c) and

$$\int_{\Omega} \Delta u \Delta v \, dx = \int_{\Omega} qv \, dx, \ \forall v \in \mathcal{H}_{D}^{2}(\Omega).$$
 (2)

The challenge is then to decide the load function q and the boundary functions f and h based on point data given either as equality or inequality constraints:

$$u(\xi_i) = d_i \text{ for } i \in \mathcal{E},$$
 (3a)

$$u(\xi_i) > d_i \text{ for } i \in \mathcal{I},$$
 (3b)

where  $\xi_i \in \Omega$  and  $\mathcal{E}$  and  $\mathcal{I}$  are finite sets of indices. Furthermore, the surface values may be known at a set of curves in the domain:

$$u = u_e \text{ on } \Gamma_e \subset \Omega.$$
 (4)

In Sec. 3 we describe a procedure for using point data (3) to obtain parameters of a load function q model. In the case, when the resulting surface is of importance only in a small subarea of the domain in which all point data is available, the effect of the boundary values can be neglected. For the other case, we describe in Sec. 4 how missing Dirichlet boundary data (1b) can be constructed from information at a set of curves, as expressed in (4). Both procedures are applied to an example from soil science, described in the next section.

#### 1.2 Organization of the paper

The topic of this paper is to cover two aspects of surface construction by an PDE approach: In Sec. 3 we focus on the load vector as a modeling parameter. Inner point constraints are used to optimally fit these parameters while in Sec. 4 given curve data is used to determine values for Dirichlet boundary conditions of the desired surface. The domains can be geometrically complex in general, while the approach of including boundary data as modeling parameters allows for simplifications of the domain to simple rectangles. Both aspects of surface construction are inherent in the surface construction problem from geoscience introduced in Sec. 2 and used to demonstrated the modeling approaches in Secs. 3 and 4. The corresponding software tools are presented in Sec. 5.

## 2 Case study: Soil thickness and bedrock surface over a region in Norway

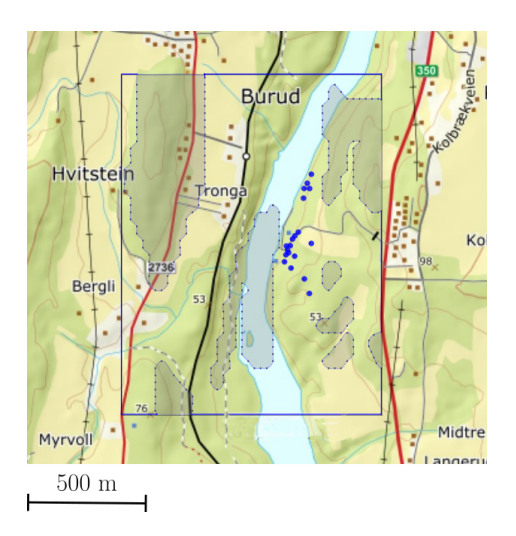


Figure 1: A part of the Norwegian region Øvre Eiker with the subregion marked for which the soil thickness is determined, [14] region: EU89 UTM33 (6639960 N, 212750 E). The position of the wells (point data) is indicated by blue circles and the exposed bedrock  $\Omega_{\rm e}$  is indicated by slightly grayed areas.

Consider a given rectangular geographical area  $\Omega_{\rm m}$  with a subarea,  $\Omega_{\rm c}$ , covered by soil. In the remaining part of the area,  $\Omega_{\rm e} := \Omega_{\rm m} \backslash \Omega_{\rm c}$ , the bedrock is exposed, cf. Fig. 1. Correspondingly, let  $u_{\rm m}$  be the terrain surface elevation,  $u_{\rm s}$  the soil thickness and  $u_{\rm b}$  the bedrock surface elevation, thus

$$u_{\rm b} = u_{\rm m} - u_{\rm s}, \quad \text{in} \quad \Omega_{\rm m},$$
 (5)

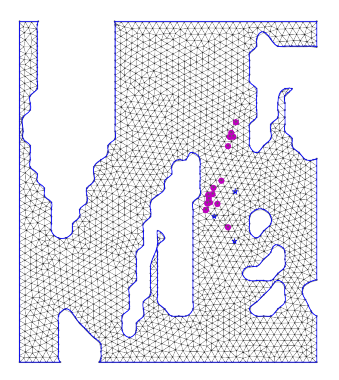
with  $u_s = 0$  in the exposed area  $\Omega_e$ .

We access the terrain surface data from the database [15] and the location of the exposed bedrock from [13]. Information about soil thickness and bedrock morphology is relevant for many different applications (viz. agriculture; hydrology, structural engineering). In this work, soil thickness will be modelled based

on local point information. Bedrock morphology will be modelled based on information about the elevation of the exposed bedrock area, in particular on the intersections between the exposed and the covered regions.

The point data that will be used in (3) are the locations and depths of wells drilled in  $\Omega_c$ . It can be retrieved from a public database [6]. When a well is drilled down to the bedrock, the soil thickness  $u_s$  is known at that point, satisfying the equality constraint (3a). The inequality constraints (3b) refer in this context to wells that do not reach entirely down to the bedrock. These data will be used in Sec. 3 to construct a surface representing the soil thickness.

The terrain surface  $u_{\rm m}$  is known over the entire domain  $\Omega_{\rm m}$ , so are the Dirichlet boundary conditions f in (1b) on the boundaries between the exposed and the covered regions in Sec. 3. In Sec. 4, these boundaries will act as the set of curves  $\Gamma_{\rm e}$  in (4), and will be used to retrieve the unknown Dirichlet boundary values at the part of the boundaries covered by soil. Hence we consider two different domains to formulate the problem: In Sec. 4 the domain  $\Omega$  is completely defined by the rectangular map section  $\Omega_{\rm m}$ . Here, the boundary is given by the edges of the rectangle. In Sec. 3 the domain is defined as  $\Omega := \Omega_{\rm c}$ . It is derived from the map section by cutting out regions with exposed bedrock. The edges of those parts together with the edges of the rectangular map form the boundary of  $\Omega_{\rm c}$ . In Fig. 2 these two domains are shown together. One sees how the more complex domain geometry when the exposed areas are removed from the domain, affects the mesh.



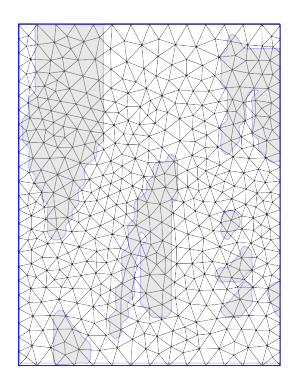


Figure 2: Two alternatives to define the underlying domain together with an automatically generated grid. *Left:* An irregular domain defined by a rectangular map segment where regions with exposed bedrock are excluded. The location of wells is marked by magenta circles and blue stars. *Right:* The same rectangular map segment including regions with exposed bedrock (shaded).

The aim is to reproduce a smooth large-scale trend of the soil thickness  $u_s$  and the bedrock surface  $u_b$ . Different approaches of modelling the soil thickness and the bedrock surface have been suggested before. An example is modeled

hill slope sediment thickness using analytical solution of differential equations, viewing sediment transport as a diffusive process, [17]. For a Poisson equation based surface model to describe soil thickness we refer to [10]. Further references to this problem can be found in [11].

## 3 Modelling the load function from point data

In this section, we describe a procedure for using point data (3) to model a load function q in the biharmonic equation (1). In this case, the boundary conditions in (1b) are assumed to be known, such that the smooth surface is given as the solution u of the discrete biharmonic equation. The procedure is then applied to the soil thickness problem described in Sec. 2.

The general idea can be described as follows: Let q be a weighted sum of load functions  $q_j$  representing each data point, thus  $q = \sum_{j=1}^{n_q} p_j q_j$ . In the current work, these are chosen in relation to the locations  $\xi_j$  of the point data as

$$q_j(x) = \frac{1}{\sigma_j \sqrt{2\pi}} e^{-\frac{1}{2}(\frac{x-\xi_j}{\sigma_j})^2}, \qquad j \in \mathcal{E} \cup \mathcal{I}.$$
 (6)

These functions respect local information, and the choice of the localization parameters  $\sigma_j$  controls the region of their influence. Let  $u_j$  be the solutions of the biharmonic equations  $\Delta^2 u_j = q_j$  with homogeneous Dirichlet boundary conditions for each of the basis functions  $q_j$ ,  $j = 1, \ldots, n_q$ . For a given function  $q = \sum_{j=1}^{n_q} p_j q_j$  with weights  $p = (p_1, \ldots, p_{n_q})$  the solution of the biharmonic equation (1) is

$$u(x;p) = \sum_{j=1}^{n_q} p_j u_j(x) + u_{\rm bc}(x), \tag{7}$$

where  $u_{\rm bc}$  is the solution of  $\Delta^2 u_{\rm bc} = 0$  respecting the given boundary conditions. The challenge is then to decide on the weight vector p. In this work, p is found by solving the following minimization problem:

$$\min_{p \in \mathcal{B}} \sum_{i=1}^{n_q} (d_i - u(\xi_i; p))^2$$
 (8a)

subject to

$$u(\xi_i; p) = d_i \text{ for } i \in \mathcal{E},$$
 (8b)

$$u(\xi_i; p) \ge d_i \text{ for } i \in \mathcal{I},$$
 (8c)

where  $\mathcal{B}=[a_1,b_1]\times\cdots\times[a_{n_q},b_{n_q}]$ , with  $[a_i,b_i]$  bounding the weight  $p_i$ , respectively. A suitable choice of bounds has to be considered to ensure that the surface generated by the biharmonic equation (1) interpolates the specified equality data points (8b), without necessarily interpolating the inequality points, and at the same time to control the smoothness of the surface to suppress possible unwanted oscillations. Without bounds, the solution will interpolate all data points, which is not the intention. The exact choice of the bounds depends on the actual application.

### 3.1 Case study: Modelling soil thickness

We will now apply the procedure described above to derive a surface mimicking the soil thickness  $u_s$  by using information from the wells as point data, as described in Sec. 2. The computational domain is restricted to the area covered by soil, thus  $\Omega = \Omega_c$ . The solution u represents the soil thickness  $u_s$ . At the boundaries between the exposed and the covered regions, the soil thickness is obviously zero. Thus, these boundaries form the Dirichlet boundary  $\partial \Omega_D$ , and u and  $\partial_n u$  are set to be zero. On the remaining parts of the boundary information is missing; these boundaries are chosen as zero Neumann boundaries  $\partial \Omega_N$  (1c). The data set consists of information from twenty wells. The distribution of the wells is visualized in Fig. 3. Only three of the wells are drilled down to the bedrock, here the soil thickness  $d_i$ ,  $i \in \mathcal{E}$  is known. This is expressed by equality constraints (3a), the blue diamonds in Fig. 3. For the remaining wells, the soil thickness is larger than the well depth  $d_i$ ,  $i \in \mathcal{I}$ , so information from them is expressed by inequality constraints (3b). The corresponding well depths are represented by magenta dots in Fig. 3.

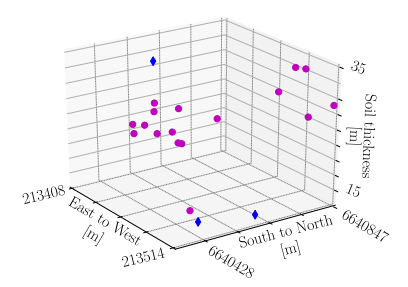


Figure 3: Distribution of the point data. Exact soil thickness (equality constraints) •. Lower bound of soil thickness (inequality constraints) •.

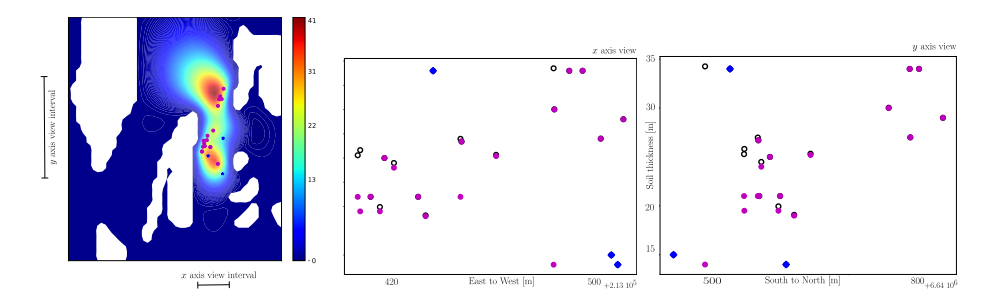


Figure 4: *Left:* Surface produced from the well data. *Right:* Measured and simulated point data, seen from the north-south axis and seen from the east-west axis: Given soil thickness •, well depths (lower bound of soil thickness) •, simulated soil thickness •.

One example of a surface constructed from the well data is depicted in Fig. 4, to the left. In this example, the localization parameters in (6) are set to  $\sigma_i = 1.5$ for all points  $\xi_i$ . Suitable bounds for the weights are chosen experimentally to  $p_i \in [0,2]$  for  $i \in \mathcal{E}$  and  $p_i \in [-1,1]$  for  $i \in \mathcal{I}$ . The discrete biharmonic equation is constructed by the Virtual Element Method (VEM) on the grid given in Fig. 2, to the left. All the measured values  $(\xi_i, d_i)$  as well as the simulated values  $(\xi_i, u(\xi_i, p))$  are presented in Fig. 4, to the right, confirming that all the constraints are satisfied.

This approach uses the local information from the wells to give a rough estimate on the soil thickness in a small subdomain that contains all wells. The smaller this subdomain the less is the influence of the outer boundary data, that normally is unknown. In contrast, the next section suggests a technique to estimate boundary data from inner curves. These are the boundary lines between the exposed and the unexposed bedrock, which will be used to estimate the bedrock topography over a larger area.

### 4 Modelling outer boundaries from inner curve data

We consider now the case of constructing boundary conditions from given data on a set of curves  $\Gamma_{\rm e} \subset \Omega$  while data on the boundary is not completely available. In particular we consider (1) as a pure Dirichlet problem with f and h being unknown on the entire boundary  $\partial\Omega_{\rm D}$  or parts of it. Again, the application presented in Sec. 2 serves as a case study after a solution method has been presented.

The problem is formulated as follows: Given two functions  $u_{e_1}$  on  $\Gamma_{e_1} \subseteq \Gamma_{e_1}$ and  $u_{e_2}$  on  $\Gamma_{e_2} \subseteq \Gamma_e$  find  $u \in \mathcal{H}^2(\Omega)$  such that

$$\int_{\Omega} \Delta u \Delta v \, dx = \int_{\Omega} qv \, dx, \ \forall v \in \mathcal{H}^{2}_{D}(\Omega)$$

$$u = u_{e_{1}} \text{ on } \Gamma_{e_{1}}$$

$$\partial_{n} u = u_{e_{2}} \text{ on } \Gamma_{e_{2}}.$$
(9a)
$$(9b)$$

$$u = u_{e_1} \text{ on } \Gamma_{e_1}$$
 (9b)

$$\partial_n u = u_{e_2} \text{ on } \Gamma_{e_2}.$$
 (9c)

This formulation is too general to allow a statement about its well-posedness. Indeed, inconsistent choices of the sets  $\Gamma_{e_1}$  and  $\Gamma_{e_2}$  might result in a problem without a solution. But it may still be possible to find a solution of its discretized counterpart, which will be used in Sec. 4.1.

On the other hand, given that a solution of (9) exists, it defines the unknown boundary functions by

$$f := u|_{\partial\Omega_D}$$
 and  $h := \partial_n u|_{\partial\Omega_D}$ .

Note that, the well posed problem (1) is a special case of (9) with  $\Gamma_{e_1}$  =  $\Gamma_{e_2} = \partial \Omega_D$ .

#### 4.1 The discrete inverse problem

A discrete formulation of problem (9) can be obtained by a Ritz ansatz with an  $n_{\text{dof}}$ -dimensional function space  $\mathcal{V}^h = \text{span}\{\phi_1, \cdots, \phi_{n_{\text{dof}}}\} \subset \mathcal{H}^2(\Omega)$  and a subspace  $\mathcal{V}_{\mathrm{D}}^{h} = \{\phi \in \mathcal{V}^{h} : \phi = 0 \text{ and } \partial_{n}\phi = 0 \text{ on } \partial\Omega_{\mathrm{D}}\} \subset \mathcal{H}_{\mathrm{D}}^{\mathrm{adol}}(\Omega)$ . Typically, the basis functions are functions with local support as used by the finite element method or the virtual element method. We denote the set of the indexes of the basis functions  $\phi_j \in \mathcal{V}_D^h$  by  $\mathcal{J}$  and their total number by  $|\mathcal{J}|$ . Furthermore we choose a discrete set of points on the inner curves,  $\{\xi_l\}_{l=1}^n \subset \Gamma_e$ . The discrete solution of (9) is

$$u^h := \sum_{j=1}^{n_{\mathrm{dof}}} c_j \phi_j$$

with coefficients  $c_i$  defined by the solution of the linear equations system:

$$\sum_{j=1}^{n_{\text{dof}}} \left( \int_{\Omega} \Delta \phi_j \Delta \phi_i \, dx \right) c_j = \int_{\Omega} q \phi_i \, dx, \qquad \text{for } i \in \mathcal{J},$$
 (10a)

$$\sum_{j=1}^{n_{\text{dof}}} \phi_j(\xi_l) c_j = u_{e_1}(\xi_l), \quad \xi_l \in \Gamma_{e_1}, \qquad l = 1, \dots, n,$$
 (10b)

$$\sum_{j=1}^{n_{\text{dof}}} \phi_j(\xi_l) c_j = u_{e_1}(\xi_l), \quad \xi_l \in \Gamma_{e_1}, \qquad l = 1, \dots, n,$$

$$\sum_{j=1}^{n_{\text{dof}}} \partial_n \phi_j(\xi_l) c_j = u_{e_2}(\xi_l), \quad \xi_l \in \Gamma_{e_2}, \qquad l = 1, \dots, n$$
(10b)

or in more compact form

$$\underbrace{\begin{pmatrix} A_1 \\ C_1 \\ C_2 \end{pmatrix}}_{A} c = \underbrace{\begin{pmatrix} b^{\text{I}} \\ b^{\text{B}} \end{pmatrix}}_{b} \tag{11}$$

with  $A_1 \in \mathbb{R}^{|\mathcal{J}| \times n_{\text{dof}}}$ ,  $C_1 \in \mathbb{R}^{n \times n_{\text{dof}}}$ , and  $C_2 \in \mathbb{R}^{n \times n_{\text{dof}}}$ . The stiffness matrix  $A_1$ is the discrete counterpart of the biharmonic differential operator.

We will first consider the quadratic case,  $n = (n_{\text{dof}} - |\mathcal{J}|)/2$ , where the amount of data from inner points matches the missing amount of data on the boundary. By solving the above system (11) the required coefficients  $c = (c_j)_{j=1}^{n_{\text{dof}}}$ and hence  $u^h$  are obtained. This will also give the boundary data

$$f := u^h_{|_{\partial\Omega_D}} \quad h := \partial_n u^h_{|_{\partial\Omega_D}}$$

resulting in the well-posed Dirichlet problem (1).

However, as already mentioned, the continuous problem (9) might have no solution and even in the case it has a unique solution the problem is ill-posed, [12]. In the discrete case, this is reflected by an ill-conditioned linear system, i.e., the matrix A in (11) is near to a rank-deficient matrix. Regularization techniques can be applied to make the solution more robust with respect to small data changes. They are based on introducing additional assumptions or constraints. Here we suggest the truncated singular value decomposition as a regularization method. Ambiguities caused by poor or missing data are removed by asking for a minimal norm solution in a lower dimensional subspace. Other regularization approaches can be found in [7] and the references therein.

We use the best rank-k approximation  $A_k$  of A and compute the unknown coefficients by

$$c_k = A_k^{\dagger} b \tag{12}$$

with  $A_k^{\dagger}$  being the Moore-Penrose inverse of  $A_k$ .

For this end we compute the singular value decomposition  $A = U\Sigma V^T$  and replace its  $n_{\text{dof}} - k$  smallest singular values by zero to obtain  $A_k$ . The regularization parameter k must be determined. It controls the trade-off between the norm of the truncated solution and the norm of the corresponding residual:

$$||c_k||_2^2 = \sum_{j=1}^k \frac{(u_j^{\mathrm{T}}b)^2}{\sigma_j^2}, \quad ||b - Ac_k||_2^2 = \sum_{j=k+1}^{n_{\mathrm{dof}}} (u_j^{\mathrm{T}}b)^2$$
 (13)

Here,  $u_i$  is the *i*-th left singular vector corresponding to the singular value  $\sigma_i$ , see, e.g. [19]. An optimal truncation parameter k can be obtained by using an L-curve method, which involves relating the two norms in (13) for varying values of k, [1, 8].

### A synthetic example

In the following example we illustrate the relation of the condition of the linear problem (11) to the distance of the inner curve  $\Gamma_{\rm e}$  from the boundary  $\partial\Omega_{\rm D}$ . Additionally it demonstrates the relation between condition number and grid granularity.

Consider the following problem

$$\Delta^2 u = 0.1 \qquad \text{in } \Omega = [0, 2] \times [0, 2] \qquad (14a)$$

$$u = u_{e_1} \qquad \text{on } \Gamma_{e_1} \qquad (14b)$$

$$\partial_n u = 0 \qquad \text{on } \Gamma_{e_2} := \partial \Omega \qquad (14c)$$

$$u = u_{e_1}$$
 on  $\Gamma_{e_1}$  (14b)  
 $u_n u = 0$  on  $\Gamma_{e_2} := \partial \Omega$  (14c)

$$\partial_n u = 0$$
 on  $\Gamma_{\mathbf{e}_2} := \partial \Omega$  (14c)

where  $u_{e_1}$  is the solution of the corresponding problem with homogeneous boundary conditions restricted to  $\Gamma_{e_1}$ , the boundary of a centered inner square with side length 2r < 2, cf. Fig. 5.

This problem has a unique solution, but it is ill-conditioned [12]. The discrete solution space  $\mathcal{V}^h$  is obtained by applying the virtual element method (VEM) using DUNE, [2], on a triangular mesh constructed from an  $n_x \times n_x$  grid,  $n_x$ being the number of intervals in each direction. Here, missing boundary data is replaced by data from equally distributed points on the inner curve, see Fig. 5. In the case of  $n_x = 8$  there are  $n_{\text{dof}} = 451$  degrees of freedom and the missing data is obtained from 32 points on the inner curve, Fig. 5.

Results are shown in Fig. 6. The picture to the left shows for  $n_x = 8$  how the condition number depends on the distance between the outer boundary and

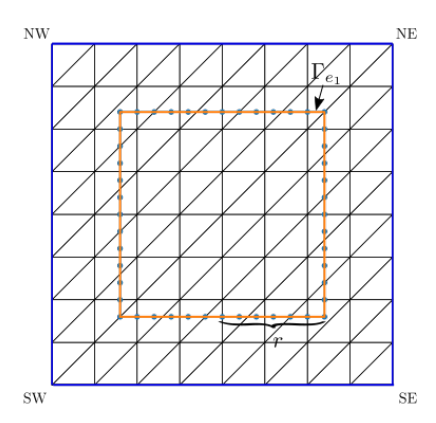


Figure 5: Domain  $\Omega$  with an inner curve  $\Gamma_{e_1}$ , forming a square of side length 2r, discretized with 32 points. The background grid is  $n_x \times n_x$  with  $n_x = 8$ .

the inner curve. As expected, the condition number decreases as the side length of the inner curve increases and thus approaches the boundary. The picture to the right shows how the condition number increases as the mesh is refined. The curves show the condition numbers for different values of  $n_x$  for the two cases: r=0.7 and r=1, the latter is the solution of the biharmonic equation in the classical case, with the outer boundary values known. The condition number in the case of r=0.7 increases much faster with  $n_x$ . Especially, when the inner curve is far from the outer boundary, a regularization technique has to be applied when solving the linear system (11).

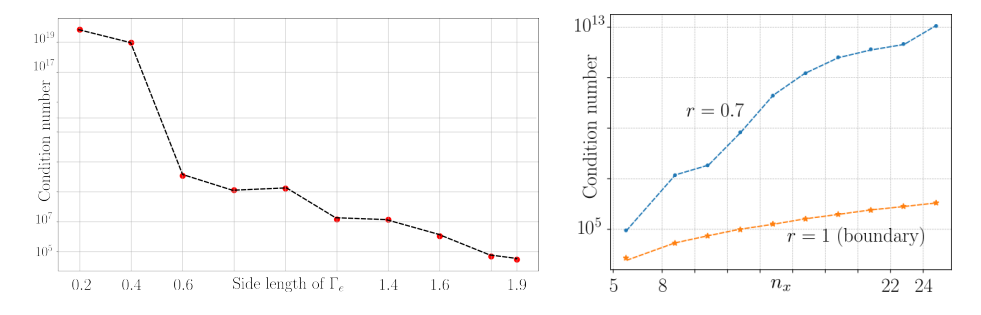


Figure 6: Left: The condition number  $\kappa(A)$  vs. the side length 2r of the inner curve. Right: The condition number  $\kappa(A)$  vs. the number of intervals in each direction  $n_x$  in the cases where r = 0.7 and r = 1.0.

Fig. 7 illustrates for problem (14) the relation between the norms of solution and residual for different truncation parameters k resulting in an L-shaped curve. Here, one observes a reduction of the norm of the solution together with an

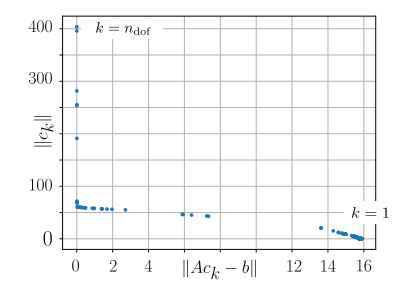
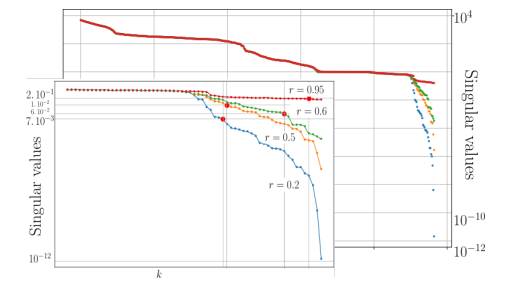


Figure 7: Illustration of the norm of the truncated solution plotted against the norm of the resulting residual for truncation parameters  $k \in \{1, 2, \dots, n_{\text{dof}} = 451\}$ 

.

increase of the norm of the residual when k decreases.

In Fig. 8 the singular values of A are traced for different values of r. One can clearly observe that most singular values are largely unaffected by the distance of the inner curve from the boundary. However, beyond a certain value of k they drop to different levels. The embedded figure focuses on this region and indicates for each test case a choice of the regularization parameter k. The influence of the size of the inner square  $\Gamma_{e_1}$  on the computed the boundary data is shown in Fig. 8 (right). Recall that as  $u_{e_1}$  was constructed from homogeneous boundary conditions, the figure shows the residual of the reconstruction experiment.



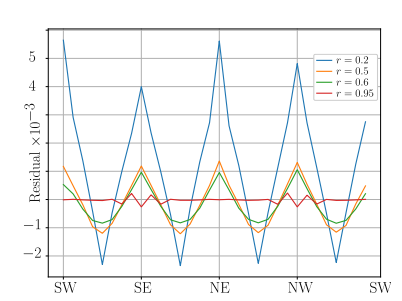


Figure 8: Left: The singular values of the system matrix for square inner curves with different side lengths 2r. The embedded graph shows a zoom of relevant region with the smallest singular values and optimal truncation point in red. Right: Residual for different inner curves  $\Gamma_{e_1}$ . It is the computed value on the boundary  $\partial\Omega_D$ .

### 4.1.2 Case study: Modelling bedrock topography

We return to the guiding example, presented in Sec. 2, and compute the soil thickness by first computing the surface of the bedrock. The reason for this

is that all subregions with exposed bedrock deliver data about the bedrock topography. That is the reason why we here formulate the problem on the domain defined by the entire map region,  $\Omega := \Omega_{\rm m}$ . For simplicity we assume that the second Dirichlet boundary condition is given by h=0, thus  $u_{\rm e_2}=0$  and  $\Gamma_{\rm e_2}=\partial\Omega$  and q=0 in (9b). Again, we aim for constructing the boundary function f. In the boundary segments intersecting with exposed bedrock,  $\partial\Omega\cap\Omega_{\rm e}$  this function is defined from the known bedrock topography, while on the remaining parts of the boundary we use available data from inner curves that is in this case topographic data from the boundaries of the exposed bedrock regions,  $\partial\Omega_{\rm e}$ .

The amount of unknowns on the boundary depends on the mesh. We can pick the same amount of data in a strategic way from these inner curves and an even more promising approach is to set up an overdetermined problem by picking more data than needed from all inner curves near the boundary,  $\partial\Omega$ .

We demonstrate this here by considering an unstructured triangular mesh of the domain  $\Omega$  generated by Gmsh, Fig. 2 (right). It consists of 531 nodes, 1514 edges and 984 triangular elements. For setting up the finite-dimensional function space  $\mathcal{V}^h$  we used an virtual element approach (VEM). The numbers of degrees of freedom is determined in this approach by the relation

$$n_{\text{dof}} = n_{\text{nodes}} \cdot 3 + n_{\text{edges}} \cdot [(\text{order} - 3) + (\text{order} - 2)] + n_{\text{elements}} \cdot (\text{order} - 3).$$

We use a third order approach which results in  $n_{\text{dof}} = 3107$  degrees of freedom. From these the desired surface is shaped. The values at all 76 boundary nodes are generated from inner curves  $\Gamma_{e_1}$  that separate exposed from covered bedrock regions in the domain or any curve within the exposed region. By taking 142 points instead, the discrete problem (11) becomes overdetermined with dimensions  $n_{\text{dof}} = 3107$ ,  $|\mathcal{J}| = 2955$ , n = 142.

The singular values of A range from  $\sigma_{\rm max}=20.64$  to  $\sigma_{\rm min}=5.14\times 10^{-7}$ . The L-curve method determines the truncation parameter k=3024 that corresponds to the singular value  $\sigma_k=4.79\times 10^{-4}$ .

By (12) the minimal norm least squares solution is obtained, from which also the boundary values can be determined, Fig. 9 (right).

Once the bedrock topography elevation is computed, we assess its physical realism by comparing it with the available terrain elevation data.

As can be seen in Fig. 10, the bedrock topography on the boundary coincides with the terrain along exposed region portions of the boundary. In the rest of the places, as there are sediments, the bedrock topography lies strictly below the terrain topography.

## 5 Software aspects

In this section we describe the software tools used for computations in the soil thickness example. The approach of using the discrete biharmonic equation requires several practical steps. For most of them ready-to-use software is available. In some steps a special adaptation of existing software is necessary.

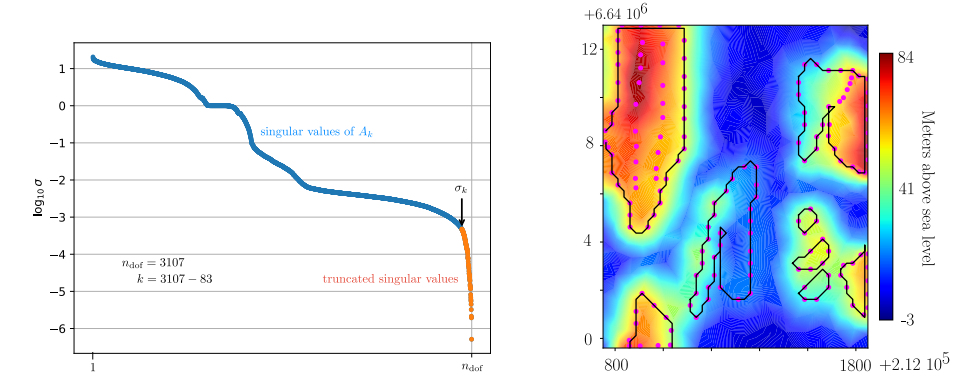


Figure 9: Bedrock topography discrete model: Left: Singular values of A and  $A_k$ . Right: Computed bedrock topography obtained by a regularization based on truncating the 83 smallest singular values. The inner data points used are indicated by dots.

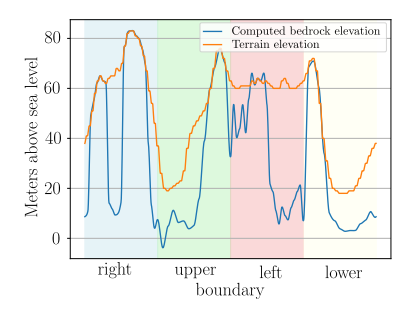


Figure 10: Computed boundary values versus terrain elevations, cf. boundary in Fig. 9 (right) in counter clockwise direction.

The data acquisition step collects data describing the domain and measurements from public sources. The Python data analysis library Pandas, [18] makes this data available for a domain description and meshing in Python. The domain is defined as a rectangular geographical region from which in Sec. 3 the areas with exposed bedrock had to be excluded. The boundaries of these areas are obtained by determining the level set curves between the exposed region and the covered region by tools from the Python library Matplotlib. On this domain a triangular mesh is generated by pygmsh, a Python wrapper of gmsh, [5].

The mesh granularity highly affects computational complexity. It serves to define the surface modeling space  $\mathcal{V}^h$ . In contrast to the situation in PDE numerics the choice of the mesh granularity is not based on accuracy requirements when seeking a solution of a PDE. It is rather a design parameter for shaping the surface. This is essential when deciding on numerical algorithms as especially

the algorithms from linear algebra used in this context have a computational complexity that grows cubically with the dimension.

To formulate the biharmonic equation on that domain and to set up the discrete formulation of (1) the modular toolbox for solving partial differential equations DUNE [2] is used. It has tools to interface with the mesh data and a mesh-to-DGF converter to mark the different boundary segments.

Our intention is to generate a smooth surface by  $\mathcal{C}^1$  functions. For this end the DUNE module dune-vem is used to set up the discrete function spaces by a third order virtual element approach, [3, 20]. This method is an off-spring of the classical finite element method, that allows to solve the biharmonic equation but with less degrees of freedom than a finite element approach with the same order would have needed. Thus, the VEM generated matrices are of smaller dimension, which leads to a higher computational efficiency.

In Sec. 4, DUNE is used to generate the system matrices and vectors in (11). From that, the solution of the discrete problem is computed outside of DUNE by the use of the Python module scipy.linalg.

The results are visualized by graphical tools provided by DUNE and the Python module matplotlib.

## 6 Summary

In this paper strategies for construction surfaces as solutions of the discrete biharmonic equation based on a rather small amount of data have been presented. These strategies result in methods which have been implemented based on standard free software. The ideas are quite general, and the solutions depend on choice of load functions, parameters and the choice of data points on inner curves, which we believe make them applicable to a larger set of situations. In this paper the strategies have been demonstrated on a concrete problem from soil science to construct surfaces mimicking some trends in soil thickness locally on covered areas, as well as the bedrock topography over a larger domain. The results are very useful as basis for further refinement of the physical results by use of geostatistical means.

## Acknowledgement

We want to acknowledge the opportunity to have many inspiring discussions with our colleagues Markus Grasmair, Robert Klöfkorn, Andreas Dedner, Alemayehu Adugna, and Zerihun Knife.

### Conflict of interest

The authors declare that they have no conflict of interest.

## References

- [1] Aburidi, M.J.: A comparative study of the regularization parameter estimation methods for the eeg inverse problem. Ph.D. thesis (2016)
- [2] Bastian, P., Blatt, M., Dedner, A., Dreier, N.A., Engwer, C., Fritze, R., Gräser, C., Grüninger, C., Kempf, D., Klöfkorn, R., Ohlberger, M., Sander, O.: The DUNE framework: Basic concepts and recent developments. Computers & Mathematics with Applications 81, 75–112 (2021). DOI https://doi.org/10.1016/j.camwa.2020.06.007. URL https://www.sciencedirect.com/science/article/pii/S089812212030256X
- [3] Brezzi, F., Marini, L.D.: Virtual element methods for plate bending problems. Computer Methods in Applied Mechanics and Engineering 253, 455– 462 (2013)
- [4] Claisse, A., Frey, P.: A nonlinear pde model for reconstructing a regular surface from sampled data using a level set formulation on triangular meshes. Journal of Computational Physics **230**(12), 4636–4656 (2011)
- [5] Geuzaine, Christophe and Remacle, Jean-Francois: Gmsh. URL http://http://gmsh.info/
- [6] Geological survey of Norway, GRANADA national groundwater database. URL http://geo.ngu.no/kart/granada/. Accessed:2024-05-29
- [7] Hansen, P.C.: Regularization tools: A matlab package for analysis and solution of discrete ill-posed problems. Numerical algorithms  $\mathbf{6}(1)$ , 1–35 (1994)
- [8] Hansen, P.C.: The L-curve and its use in the numerical treatment of inverse problems. IMM, Department of Mathematical Modelling, Technical University of Denmark (1999)
- [9] Kazhdan, M., Bolitho, M., Hoppe, H.: Poisson surface reconstruction. In: K. Polthier, A. Sheffer (eds.) Proceedings of the fourth Eurographics symposium on Geometry processing, vol. 7 (4) (2006)
- [10] Kitterød, N.O.: Estimating unconsolidated sediment cover thickness by using the horizontal distance to a bedrock outcrop as secondary information. Hydrology and Earth System Sciences 21(8), 4195–4211 (2017)
- [11] Kitterød, N.O., Leblois, É.: Estimation of sediment thickness by solving poisson's equation with bedrock outcrops as boundary conditions. Hydrology Research **52**(3), 597–619 (2021)
- [12] Lesnic, D., Elliott, L., Ingham, D., Zeb, A.: A numerical method for an inverse biharmonic problem. Inverse Problems in Engineering **7**(5), 409–431 (1999)

- [13] Unconsolidated deposits national database. URL http://geo.ngu.no/kart/losmasse. Accessed 29.05.2024
- [14] Norwegian Mapping Authority: URL https://norgeskart.no. Accessed: 2024-05-29
- [15] Norwegian Mapping Authority: Elevation data. URL https://hoydedata.no/LaserInnsyn2. Accessed 29.05.2024
- [16] Piegl, L., Tiller, W.: The NURBS Book. Monographs in Visual Communicatio. Monographs in Visual Communication. Springer (2000)
- [17] Rempe, D., Dietrich, W.: A bottom-up control on fresh-bedrock topography under landscapes. Proceedings of the National Academy of Sciences 118(18), 6576–6581 (2014). URL https://www.pnas.org/doi/full/10.1073/pnas.1404763111
- [18] pandas development team, T.: pandas-dev/pandas: Pandas (2020). DOI 10.5281/zenodo.3509134. URL https://doi.org/10.5281/zenodo.3509134
- [19] Trefethen, L.N., Bau, D.: Numerical Linear Algebra. SIAM (1997)
- [20] Beirão da Veiga, L., Brezzi, F., Cangiani, A., Manzini, G., Marini, L.D., Russo, A.: Basic principles of virtual element methods. Mathematical Models and Methods in Applied Sciences 23(01), 199–214 (2013)